HHS Public Access

Author manuscript

Mol Pharm. Author manuscript; available in PMC 2016 October 07.

Published in final edited form as:

Mol Pharm. 2015 December 7; 12(12): 4237–4246. doi:10.1021/acs.molpharmaceut.5b00430.

Protonation and Trapping of a Small pH-Sensitive Near-Infrared Fluorescent Molecule in the Acidic Tumor Environment Delineate Diverse Tumors In Vivo

Rebecca C. Gilson[†,‡], **Rui Tang**[†], **Avik Som**[†,‡], **Chloe Klajer**[†], **Pinaki Sarder**[†], **Gail P. Sudlow**[†], **Walter J. Akers**[‡,†], and **Samuel Achilefu**[*,†,‡,‖]

[†]Department of Radiology, Washington University in St. Louis, St. Louis 63110, United States

[‡]Department of Biomedical Engineering, Washington University in St. Louis, St. Louis 63110, United States

[‖]Department of Biochemistry & Molecular Biophysics, Washington University in St. Louis, St. Louis 63110, United States

Abstract

Enhanced glycolysis and poor perfusion in most solid malignant tumors create an acidic extracellular environment, which enhances tumor growth, invasion, and metastasis. Complex molecular systems have been explored for imaging and treating these tumors. Here, we report the development of a small molecule, LS662, that emits near-infrared (NIR) fluorescence upon protonation by the extracellular acidic pH environment of diverse solid tumors. Protonation of LS662 induces selective internalization into tumor cells and retention in the tumor microenvironment. Noninvasive NIR imaging demonstrates selective retention of the pH sensor in diverse tumors and two-photon microscopy of *ex vivo* tumors reveals significant retention of LS662 in tumor cells and the acid tumor microenvironment. Passive and active internalization processes combine to enhance NIR fluorescence in tumors over time. The low background fluorescence allows detection of tumors with high sensitivity, as well as delineation of dead or dying cells from healthy cells. In addition to demonstrating the feasibility of using small molecule pH sensors to image multiple aggressive solid tumor types via protonation-induced internalization and retention pathway, the study reveals the potential to use LS662 for monitoring treatment response and tumor-targeted drug delivery.

Keywords

cancer imaging; fluorescence; small animal; tumor model; extracellular pH; pH-sensitive probe

[*]Corresponding Author: Tel (314)362-8599. achilefus@mir.wustl.edu.

Notes

The authors declare no competing financial interest

ASSOCIATED CONTENT

Supporting Information.

Synthesis, absorption And emission spectra, and *in vivo* distribution of LS798.

This information is available free of charge via the Internet at http://pubs.acs.org/.

Introduction

Aggressive solid tumors utilize enhanced glycolysis for energy production and proliferation, leading to a net increase in intracellular protons relative to that in healthy cells. To remain viable at a normal physiological intracellular pH (pHi) of 7.4, cancer cells actively pump out the excess protons.[1] However, the poor lymphatic function and chaotic vascularization of tumors result in an inefficient buffering or removal of the effluxed protons, leading to a significant reduction in extracellular pH (pHe) from 7.4 to 6.2–6.9.[1, 2]

Previous studies have demonstrated that the acidic pHe of solid tumors correlates with an increase in tumor invasiveness and cell proliferation, as well as a decrease in chemotherapeutic efficacy.[1, 3–6] The therapeutic effect of modulating the acidic pHe was demonstrated in preclinical models by oral administration of sodium bicarbonate, which systemically neutralized the pHe of the whole body, including tumors. The systemic neutralization reduced tumor burden and decreased the number of circulating tumor cells.[3, 4, 7–9] These results suggest that the acidic pHe of solid tumors is not only a byproduct of mitochondrial dysfunction and enhanced glycolysis,[10] but also represents an important survival pathway that supports tumor growth and metastasis. Thus, the ability to noninvasively image the pHe of tumors affords new means to determine the aggressiveness and severity of cancer or to monitor treatment response.

A variety of molecular imaging probes and nanoparticles have been developed for *in vivo* imaging of pH changes.[2, 11–14] Although chemical exchange saturation transfer (CEST) enhanced magnetic resonance imaging provides depth-independent assessment of pH *in vivo*, the method requires long acquisition times[15] and the use of high concentration of the CEST contrast agent.[16] For small animal imaging or the assessment of superficial and endoscopically accessible tumors, optical methods represent a high throughput imaging platform for real-time image display[17] and detection of pH changes *in vivo* via multiple contrast-generating molecular probe designs.

An interesting approach is the wide use of activatable molecular probes to amplify the signal-to-background ratio. This approach has been used successfully to report enzyme activities,[18–24] intracellular pH,[11–13, 25] and intracellular levels of reactive oxygen species.[26] To combine targeted delivery with fluorescence enhancement *in vivo*, recent studies have conjugated pH-sensitive dyes to tumor-targeting ligands such as RGD peptides,[11] where the progressive pH decrease along the endocytotic pathway culminates into high fluorescence in the lysosomes of tumor cells.[11–13] The pKa of pH sensors can be tuned to minimize background fluorescence in nonacidic cell compartments or tissue environment. However, tumor heterogeneity dictates significant variability in the expression of the targeted proteins in tumor cells. When conjugated to tumor-targeting ligands, the primary mode of fluorescence enhancement for the pH sensors is through intracellular acidic organelles, with limited access to the acidic extracellular tumor environment.

In this study, we have developed a pH-sensitive molecule, LS662, for noninvasive imaging of the acidic pHe of solid tumors. We demonstrate that protonation of the small NIR fluorescent molecule (~700 Da) in the mildly acidic environment of diverse solid tumor

types induces absorption spectral shift from visible to NIR region. We used the ensuing NIR fluorescence to successfully identify three different tumor models, including syngeneic and spontaneous murine and human xenograft tumors. The selective retention of LS662 in tumor cells and the acidic environment for over 3 days suggests that protonation traps the small molecule and facilitates internalization in cancer cells without conjugating the dye to a tumor-targeting protein or peptide.[11] This study demonstrates the potential use of LS662 for interrogating physiologic parameters in a broad range of cancers.

Materials and Methods

Materials

Dulbecco's modified Eagle's medium (DMEM) culture medium, fetal calf serum, and penicillin-streptomycin were purchased from Gibco, (Life Technologies, NY, USA). Vectashield was purchased from Vector Laboratories (CA, USA).

Human epidermoid cancer (A431) cells were obtained from ATCC (VA, USA) and 4T1/luc murine breast cancer cells were obtained from David Piwnica-Worms, Washington University in St. Louis.[27] Cells were cultured using DMEM supplemented with 10% FBS, and 1% penicillin streptomycin in a humidified incubator at 5% CO_2 balanced with air at 37°C. The cells were kept at 50–80% confluence.

Female BALB/c and female athymic NCr-nu/nu mice were obtained from Charles River Laboratories (MA, USA). Female PyMT mice were bred in-house. All animal studies were performed with accordance with protocols approved by the Washington University School of Medicine Animal Studies Committee.

Synthesis of pH-sensitive NIR fluorescent dye, LS662

The synthesis of LS662 is summarized in figure 2A. A mixture of Vilsmeier reagent **1** (1.1 g, 3 mmol) and 4-carboxylphenyboronic acid (1 g, 6 mmol) was heated overnight under reflux in DMF in the presence of potassium acetate (66 mg, 0.69 mmol) and tetrakis(triphenylphosphine)palladium(0) (0.22 g, 0.19 mmol). The reaction mixture was allowed to cool to room temperature and DMF was evaporated. HPLC purification of product **2** afforded 0.67 g of a blue-green solid (55% yield). A mixture of the indolenium sulfonate **3** (100 mg, 0.38 mmol) and the Suzuki product **2** (73 mg, 0.18 mmol) was heated under reflux in the presence of sodium acetate (55 mg, 0.67 mmol) in 10 mL an ethanol/acetic anhydride solution (1/1, v/v) for 20 h. After cooling, 2 mL of a 3% aqueous HCl solution was added to the resultant mixture. The crude product was purified by reverse-phase C-18 column chromatography, and the desired compound was eluted with CH_3CN/H_2O (57 mg; 45% yield; ^{1}H NMR (400 MHz, DMSO-d_6)) δ 1.26 (s, 12 H), 1.90 (m, 2H), 2.60 (m, 4H), 6.96 (d, J = 14 Hz, 2H), 7.04 (d, J = 8 Hz, 2H), 7.34 (d, J = 8 Hz, 2H), 7.52 (d, J = 8 Hz, 2H), 7.61 (s, 2H), 8.15 (d, J = 8 Hz, 2H). ESI-MS: m/z 701 (M+H, 100%).

Spectral properties and pKa of LS662

The absorption and emission spectra of LS662 were recorded on a spectrophotometer (Beckman DU640, CA, USA) and fluorometer (Fluorolog-3, Horiba Jobin Yvon, NJ, USA), respectively. Determination of the absorption and emission maxima was reported in solutions with pH values below and above 5. The fluorescence quantum yield of LS662 in PBS was determined by using a literature method and referenced to indocyanine green dye.[11] For pH titrations, LS662 was dissolved in 30 mL water. 175 mg NaCl (0.003 mmol) was added to provide relative constant ionic strength of 0.1 M. The initial solution was acidified with dilute aqueous HCl (0.1 M) to achieve pH = 2.34. The increment of the pH value was achieved by adding small amount of dilute NaOH (vary from 0.1 M to 0.0001 M) into the dye solution. The pH of the solutions were measured with a pH meter (Accumet AB15, MA, US). At each pH point, the absorption and fluorescence spectra were recorded. The pKa of LS662 was determined using sigmoidal dose-response curve fitting software (GraphPad Prism 5.0, CA, USA).

To obtain optical images of the dye at pH 6.0 and 6.5, 2-(N-morpholino)ethanesulfonic acid (MES; 1 M) was prepared in water and titrated with NaOH to the appropriate pH. For pH 7.0 and 7.5 medium, 4-(2-hydroxyethyl)-1-piperazineethanesulfonic acid (HEPES; 1 M) was prepared in water and titrated with HCl or NaOH to the appropriate pH. These solutions were diluted with phenol-red free and bicarbonate-free DMEM to obtain a final concentration of 20 mM. LS662 (10 μM) was dissolved in each solution (100 μL) in a 96-well plate and imaged on the Pearl NIR fluorescence imaging system, ex/em 785/820 nm (LICOR Biosciences, NE, USA).

Blocking and pH variable internalization

A431 cells were grown in 96 well plates (BD Biosciences, NJ, USA). The cells were treated with 1 μM of LS662 for 1–8 h, in either acidic (pH 6.4) or neutral (pH 7.4) medium. Acidic medium was made by adding 25 μL of 1 M HCl per 1 mL of medium. For blocking studies, 10 mM sodium azide, an active transport inhibitor, was co-incubated with the cells. After treatment, the cells were rinsed with PBS and imaged using a BX-51 epifluorescent microscope (Olympus, PA, USA). A cy5 U-N41008 (Chroma Technology Corp, VT, USA) filter cube was used for excitation at 620/60 nm and emission collection at 700/75 nm.

4T1/luc cells were grown in an 8 well slide (BD Biosciences, NJ, USA). The cells were treated with 10 μM of LS662 or 1 μM of cypate for 2 or 8 h, in either acidic (pH 6.4) or neutral (pH 7.4) medium. After treatment, the cells were rinsed with acidic or neutral medium and imaged using a FV1000 confocal microscope with an UPLanApo/IR 60X/ 1.20W water immersion objective lens (Olympus, PA, USA) at 633 nm (LS662) or 785 nm (cypate) excitation laser, and fluorescence was detected at 690/50 nm (LS662), or 850 LP (cypate).

Cell death assay

A431 cells were grown on an eight well microscope slides (BD Biosciences, NJ, USA). To determine if LS662 preferentially stains dead cells, three conditions of A431 cells were incubated with 1 μM LS662 or 1 μM cypate for 2 h: healthy cells (cell in medium with

LS662), dying cells (cell incubated with PBS with LS662), and dead cells (cell pretreated with 50% ethanol in PBS for 30 min, with LS662 added after the treatment with ethanol). After treatment, the cells were rinsed with PBS, mounted with Vectashield (Vector Laboratories, CA, USA), and coversliped. The slides were imaged using a FV1000 confocal microscope with an UPLanApo/IR 60X/1.20W water immersion objective lens (Olympus, PA, USA) at 633 nm (LS662) or 785 nm (cypate) excitation, and fluorescence was detected at 690/50 nm (LS662), or 850 LP (cypate).

Induction of tumors in murine models

All animal studies were performed in accordance with protocols approved by the Washington University School of Medicine Animal Studies Committee. Syngeneic 4T1/luc murine breast tumors were initiated in mice by injecting 5×10^5 4T1/luc breast cancer cells subcutaneously in the right flank of 6–8 week old female BALB/c mice. Imaging studies were performed after the tumors had grown for approximately 10 days to a size of 5–7 mm in diameter. A431 human epithelial carcinoma xenografts were grown in 6–8 week old female athymic NCr-nu/nu mice by injecting bilateral A431 cells into the mammary fat pad. Imaging studies were conducted after tumors had grown for approximately 15 days to a size of 5–7 mm in diameter. The spontaneous breast cancer mouse model expressing the polyomavirus middle T antigen via the mouse mammary tumor virus long terminal repeat promoter (PyMT) was bred in-house. Heterozygous mice developed spontaneous, multifocal mammary adenocarcinomas at about 8–12 weeks of age.

In vivo and *ex vivo* tumor imaging

LS662 or cypate, was dissolved in DMSO then diluted with PBS for a final concentration of 60 μM in 100 μL of 20% DMSO and 80% PBS. The solution was injected intravenously via the lateral tail vein. Fluorescent imaging was performed using the Pearl NIR fluorescence imaging system, ex/em 785/820 nm before injection and at 1, 2, 4, 6, 24, 48, and 72 h post injection. After 72 h, the mice were euthanized and organs of interest were removed, placed on a Petri dish, and imaged with the Pearl imager. Region of interest (ROI) analysis was performed with the Pearl imaging software. The mean fluorescence intensities were measured for each tissue to assess the biodistribution of each compound. In addition, *in vivo* ROIs for tumor and normal tissues were used to determine the accumulation of the probe over time. The normal tissue regions were chosen that did not include any excretory organs or tumors in order to obtain a reliable background measurement.

Ex vivo multiphoton imaging

After excision, tumors were cut into 1 mm slices and imaged using a custom built two-photon microscope at the Washington University School of Medicine. The visible emission from LS662 was excited with a Chameleon XR Ti-Sapphire laser (coherent) and visualized with an Olympus XLUMPlanFl 20X objective (water immersion, NA 0.95). Fluorescence emission from collagen, elastin, and LS662 was separated passing through 515 and 560 nm dichroic mirrors and detected as red (560–650 nm), green (490–560 nm) and blue (second harmonic < 458 nm) channels by three head on Bialkali photomultiplier tubes.[28, 29] Z-stack images were acquired by taking 20 sequential images at a step size of 2.5 μm, and averaged

15 video rate frames for each z-slice. Imaris (Bitplane, MA, USA) and ImageJ (NIH, MD, USA) were used for multidimensional rendering.[30]

Histological analysis

Excised tumor tissues were flash-frozen in OCT (Tissue Tek, CA, USA) and stored at −20 °C. The tumors were sliced at a thickness of 10 μm (Cryocut 1800, IL, USA). Fluorescence imaging was performed with an Olympus BX51 upright epifluorescent microscope (Olympus America, PA, USA). A cy5 U-N41008 (Chroma Technology Corp, VT, USA) filter cube was used for excitation at 620/60 nm and emission collection at 700/75 nm. Muscle samples, taken from the mouse's left leg, were imaged with the above settings as nontumor control samples. To confirm that lack of LS662 fluorescence was not due to inactivation, acidic PBS (pH 4.0) was added to the sample to activate any LS662. H&E staining of excised tumor and surrounding tissues was used for histologic validation of tissue types.

Statistical analysis

All cell studies were performed in triplicate. The mean fluorescence per image was calculated after background fluorescence subtraction and normalized to the number of cells per image. These values were then averaged and error bars represent the standard deviation. For *in vivo* quantification of tumor and normal tissue fluorescence the following number replicates were used: 3 for 4T1/luc tumor and normal, 2 A431 tumor and 3 for A431 normal, 3 for PyMT tumor and normal. For *ex vivo* quantification of tumor and muscle fluorescence the following number replicates were used: 3 for 4T1/luc tumor and muscle, 2 A431 tumor and 1 for A431 muscle, and 3 for PyMT tumor and 1 for PyMT muscle. When more than 3 replicates were present, the standard deviation was calculated and displayed as error bars. Statistical significance was calculated using the Student T-Test and p-values below 0.05, were considered statistically significant.

RESULTS

Synthesis and spectral properties of pH-sensitive NIR fluorescent dye, LS662

We have developed LS662 as a pH-sensitive small molecule for identifying tumors. Upon protonation in acidic media, the molecule undergoes significant spectral shift from visible to NIR wavelength. The high NIR fluorescence is useful for identifying diverse tumors (Figure 1).

LS662 was synthesized by modifying our previously reported method (Figure 2A).[11] To overcome the low yields, we used a modified Suzuki-coupling condition in which Vilsmeier reagent **1** was reacted with 4-carboxyphenylboronic acid in the presence of tetrakis(triphenylphosphine)palladium(0) and anhydrous potassium acetate. The purified LS662 was obtained as blue-green solid. The dye is stable in powder form; although the aqueous solution can be stored at 4 °C for several weeks, it is best to use the freshly prepared solutions for each study. pH titration show that LS662 has low NIR fluorescence in basic and neutral solutions, displaying an absorption maximum (λ_{abs}) at 503 nm (Figure 2C). A significant hypsochromic shift from 503 nm to 750 nm λ_{abs} and an intense NIR

emission maximum (λ_{em}) at 768 nm were observed in acidic solutions (pH<6), with corresponding pK_a, molar absorptivity (ε), and fluorescence quantum yield (Φ_F) of 5.2, 120,000 M^{-1} cm^{-1}, and 0.025, respectively in PBS. Protonation of one indolenium ring nitrogen in LS662 converts the molecule into a donor-acceptor fluorophore system, which exhibits a large spectral shift.[11] Pseudocolor fluorescence images of LS662 solutions in different pH buffers provide visual changes in fluorescence intensity with increase in pH (Figure 2D).

LS662 differentially internalizes in tumor cells via dual ATP-dependent and independent pathways in neutral and acidic culture media

We postulated that protonation of LS662 under mild acidic conditions found in the pHe of many solid tumors will decrease the molecule's net negative charge, enhance NIR fluorescence, and facilitate internalization in cells. To test this hypothesis, LS662 was incubated with representative tumor cells (A431 or 4T1/luc) in buffer solutions at pH 7.4 and 6.4 to simulate normal physiological and acidic tumor pHe values, respectively (Figure 3A). At pH 7.4, only a few cells exhibited high NIR fluorescence within 2 h incubation. Longer incubation times showed a weak and diffuse NIR fluorescence in nearly all cells. A similar trend was observed in acidic solutions, in which the internalization of LS662 occurred in only a few cells within 2 h of incubation, but increased significantly at 8 h measurement time point. The few cells exhibiting high NIR fluorescence within 2 h in both normal and acidic media are probably dying or dead cells. From structural consideration alone, internalization of the highly negatively charged LS662 into cells at neutral pH would not be expected because of electrostatic repulsion from cell membrane's phosphate groups. Therefore, the delayed but significant accumulation of the molecular probe in cancer cells at long incubation times suggests a molecular rearrangement that facilitates passive or active transport in cells. Compared with cells treated at pH 7.4, fluorescence of LS662 was significantly higher under acidic conditions. This internalization process could be mediated by electrostatic interactions of protonated LS662 with the phosphate groups in cell membranes (Figure 1D). As control, a less physiologically pH-sensitive dye cypate (Figure 2B),[31] was also incubated with 4T1/luc cells. As expected, the internalization of cypate was not pH dependent (Figure 3B).

To investigate the mechanism for LS662 internalization, we incubated A431 or 4T1/luc cells with the pH sensor in acidic (pHe 6.4) and neutral (pHe 7.4) media in the presence or absence of sodium azide, an active transport inhibitor (Figure 3A).[32, 33] In both acidic and neutral solutions, cells treated with sodium azide exhibited lower NIR fluorescence than the untreated control. However, the decrease in LS662 fluorescence was higher under neutral (77% A431, 32% 4T1/luc) than acidic (13% A431, 9.5% 4T1/luc) conditions at 8 h post incubation (Figure 3B). This finding suggests that the highly negatively charged, nonprotonated LS662 overcomes electrostatic repulsion at the plasma membrane via an active transport process. In the protonated form, ATP-independent endocytosis dominates LS662 internalization. Cypate internalization was not blocked by the addition of sodium azide.

Because the NIR fluorescence of LS662 is weak under neutral pH, the high intracellular fluorescence most likely occurred through the acidic endosomal pathway or by translocation into acidic intracellular organelles. Co-incubating LS662 with a lysosomal reporter, lysotracker green, showed that the punctate LS662 fluorescence co-localized with the lysotracker dye, indicating that LS662 is in the acidic lysosomes (Figure 3D).

LS662 is a highly sensitive reporter of dying and dead cells

Regardless of the treatment conditions, some cells exhibited bright LS662 fluorescence within 2 h post incubation, suggesting that the molecular probe could serve as reporter of cell death. To explore this capability, A431 cells were incubated with LS662 for 2 h under three different conditions: normal culture media, PBS solution, or 50% ethanol in PBS, to obtain predominantly healthy, dying, and dead cells, respectively (Figure 3C). Cypate was incubated with cells under similar conditions (Figure 3C). As cells die, a 5000-fold increase in LS662 fluorescence was observed, whereas the fluorescence from cypate only showed a moderate 2-fold increase. The small increase in cypate fluorescence could be attributed to nonspecific uptake in dead cells.

Previous studies have shown that cells undergoing necrosis or apoptosis are characterized by the disruption of their organelles' membranes, leading to release of their contents, and acidification of the cytosol, with fewer residual intact lysosomes.[14, 34, 35] Thus, the high increase in LS662 fluorescence in dead or dying cells suggests protonation of the molecule under the mild intracellular acidic conditions of these cells (Figure 3C). Loss of intracellular membrane integrity transforms the highly punctate LS662 fluorescence to a more diffuse intracellular pattern. These results illustrate the multidimensional use of LS662 to localize tumors and possibly to identify dying cells in response to treatment.

Protonation of LS662 enhances NIR fluorescence in mouse and human cancer models

A primary goal of this study is to evaluate the feasibility of imaging diverse solid tumors using the simple pH-sensitive molecular probe *in vivo*. Starting with subcutaneous 4T1/luc tumors in the flanks of mice, fluorescence of LS662 in the tumor region was evident as early as 1 h post injection, attaining maximum contrast at 72 h (Figure 4Ai–ii). The high tumor tissue-selective contrast was confirmed by *ex vivo* imaging and region of interest analysis of the tumor, with a tumor-to-muscle contrast of 15.7 ± 0.3 (Figure 4Aiii). The high fluorescence in the kidneys and liver suggests a bimodal excretion routes for LS662. As a small hydrophilic molecule, renal excretion was expected. The significant hepatobiliary excretion indicates that a fraction of the dye was bound to blood proteins, which then presents the molecules to the liver for subsequent excretion. The widely used NIR fluorescent dyes, ICG and cypate, are excreted from the body by a similar hepatobiliary pathway (Figure 4D).[36, 37] Low uptake in the spleen and lungs suggests minimal aggregation of the molecular probe in vivo.

We compared uptake of the pH-sensitive dye with cypate, a similar cyanine dye exhibiting less pH response.[31, 38] The longitudinal imaging of cypate in 4T1/luc tumor bearing mice shows rapid clearance from the body within 1 h post injection. The cypate fluorescence was barely detectable after 24 h post injection (Figure 4D). Quantitative image analysis shows

that there is no selective accumulation or retention of cypate in tumors. A similar result using cypate was obtained with LS798. This compound is structurally similar to LS662, but the fluorescence and absorption spectra do not respond to pH changes in the physiologically relevant range of 4–8 pH units (see Supporting Information). These results lend credence to the use of simple and small pH-sensitive NIR fluorescent dyes to interrogate the acidic milieu of solid tumors.

Having demonstrated that LS662 can localize in the acidic environment of a subcutaneously implanted murine mammary tumor model, we extended this imaging approach to the human-origin A431 tumor xenograft model (Figure 4B). The tumor cells were grown bilaterally in the mammary fat pads of athymic nude mice. Administration of LS662 in the tumor-bearing mice and subsequent fluorescence imaging showed a rapid clearance of the dye from blood and other tissue. At 1 h post injection, high fluorescence in the bladder was observed, probably due to the low pH of urine. Although the initial fluorescence was low, the accumulation and the activation of LS662 in the tumor was evident as early as 1 h post injection, culminating into maximum tumor-to-normal tissue contrast at 72 h post injection. This temporal increase suggests that the nonfluorescent LS662 remained in circulation or was already trapped in the tumor and became fluorescent with continuous protonation of the molecules. A tumor-to-muscle contrast of 14.30 ± 0.03 was determined *ex vivo* from the excised organs (Figure 4Biii).

Subcutaneously implanted tumor models do not fully recapitulate the biologic and histopathologic features of human cancers. Therefore, we explored the applicability of this approach in PyMT spontaneous murine breast cancer model. The PyMT mice are immunocompetent and present aspects of human breast cancer that are not represented by xenograft models. The similarities include spontaneous tumor development and the complex interaction of immune cells within the tumor. Intravenous administration of LS662 and fluorescence imaging showed rapid hepatobiliary clearance within 1 h post injection of LS662 (Figure 4C). This enhanced excretion pathway illustrates the variability in biodistribution that can be induced by different animal models. In this model, liver uptake was favored compared to the renal excretion observed in the subcutaneous tumor models (Figure 4A, B). Low fluorescence was observed in the tumors around the mammary fat pads, becoming more evident at 4 h before plateauing after 24 h post injection (Figure 4Cii). This model also shows lower tumor-to-muscle contrast (3.46 ± 0.19) than 4T1/luc and A431 tumor models. It is likely that the multifocal nature of the PyMT tumors prevented local concentration of secreted protons seen in the other tumors, which could minimize the extent of pHe reduction from normal physiologic pHe. In spite of relatively low tumor-to-background contrast, histologic analysis of excised suspicious tissue showed that LS662 was able to detect multiple small tumors.

Two-photon imaging and fluorescence histology reveals a punctate and diffuse intratumoral distribution of LS662

The planar NIR fluorescence imaging system we used to acquire the in vivo images is a surface-weighted low-resolution device. To determine the distribution of LS662 in the tumor microenvironment, we used high-resolution 2-photon fluorescence and second harmonic

generation microscopy for the study. The 3D reconstruction of freshly excised 4T1/luc tumor after LS662 injection reveals a chaotic structure of collagen (blue) and elastin (green) that surround and form the 4T1/luc tumor matrix (Figure 5A). LS662 (red) is distributed in the diffuse extracellular region just interior to the tumor capsule and is localized with fibrous bundles surrounding and inside the tumor. A depth of up to 100 μm was imaged, which is a typical penetration depth of 2-photon microscopy.[39] After two-photon imaging, the tumor was frozen in OCT and sectioned for histology. Imaging of the same region shows LS662 fluorescence originating from cellular regions of the tissue (Figure 5A right). The two photon images demonstrate that LS662 is able to interrogate the extracellular matrix (ECM) of tumors, with a significant fraction specifically internalizing into tumor cells.

Further analysis of the PyMT tumors via fluorescence histology shows that LS662 localized in specific cells and throughout the tumor stroma, supporting the findings from the 4T1/luc 2-photon imaging (Figure 5D). We also found that a tumor-infiltrated lymph node displayed high LS662 fluorescence (Figure 5E). Muscle samples from the left leg of the mouse were obtained from the mice to evaluate the presence of LS662 in healthy tissue (Figure 5F). Absence of NIR fluorescence indicates that LS662 is not present in normal tissue, except the excretion organs. Acidification of the muscle tissue with PBS (pH 4.0) did not display NIR fluorescence, indicating the absence of residual nonprotonated LS662 in healthy tissue.

Discussion

Previously considered a side product of enhanced glycolysis, acidification of tumor environment appears to support tumor proliferation and metastasis of aggressive solid tumors. Earlier studies have demonstrated the potential of targeting this physiologic condition for cancer detection and treatment.[3, 4, 9, 40] For optical imaging, pH-responsive molecular designs include the conjugation of pH sensors to tumor-targeting groups such as peptides or antibodies.[11] Other pH sensor design strategies include the incorporation of pH-cleavable linkers into nanoparticle constructs, followed by the release of high concentration of chemotherapeutics or imaging agents in solid tumors *in vivo*.[41, 42] Similarly, conjugation of multiple dyes to macromolecules *via* acid cleavable linkers or loading of dyes into pH-degradable nanoparticles can quench dye fluorescence, which is activated upon degradation of the product under acidic conditions.[11, 16, 41] Previously, we demonstrated that conjugation of a pH sensor to RGD peptide allowed tumor detection with high tumor-to-background fluorescence contrast. Fluorescence enhancement was generated in only intracellular compartments, similar to other receptor-targeted approaches.[11] In this study, we explored the feasibility of using a simple and small pH-sensitive molecule to image acidic pHe *in vivo*. By avoiding the complexity of nanoparticle formulations and conjugation of the pH-sensitive molecules with tumor targeting agents, LS662 represents a viable alternative to current pH-sensing molecular probes. Because LS662 possesses intrinsic tumor-targeting and retention properties, we can conjugate drugs instead of tumor-avid ligands to the free carboxylic acid moiety for targeted therapy.

The pH in the extracellular environment of tumors is generally about 6.5, whereas the pH of blood and most nontumor tissues is approximately 7.4. Because LS662 is a weak acid with a

pKa of 5.2, the Henderson-Hasselbach equation can be used to estimate the percentage of protonated LS662 at pH 6.5 *versus* pH 7.4:

$$pH = pK_a + \log_{10}\frac{[A^-]}{[HA]}$$

where $[A^-]$ and [HA] are the nonprotonated and protonated forms of LS662. Using the above equation, we expect 0.6% and 5% of protonated LS662 in the nontumor and tumor environment, respectively, representing an 8-fold increase of the protonated form in the acidic tumor environment.

We studied the relative fluorescence enhancement of LS662 in tumor versus nontumor tissues, including the *in vivo* kinetic analysis and *ex vivo* fluorescence biodistribution for all cancer models used (Figure 4). Because the pH-sensitive LS662 and the less pH-sensitive cypate (in physiologically relevant pH range) are not specifically targeted to tumor cells, we expect similar *in vivo* biodistribution profiles for both compounds. Therefore, the higher fluorescence intensity in the tumor tissues observed with LS662 is attributed to pH-dependent protonation of the dye. LS662 has a pKa of 5.2 and exhibits low fluorescence above pH 7, which provides low background signal. Although these characteristics improved the tumor-to-surrounding tissue contrast, only a small fraction of LS662 is protonated between pH 6 and 7. Increasing the proportion of protonated form of the dye in the acidic environment of tumors will improve both the tumor-to-nontumor contrast and net signal (fluorescence intensity). One approach to accomplish this goal is to develop or use a NIR fluorescent pH-sensitive dye possessing a pKa of about 6.5 and negligible fluorescence above pH 7.2.

LS662 appears to accumulate and internalize in tumor cells by a bimodal pathway. In the nonprotonated form, the highly negatively charged molecules undergo ATP-dependent endocytosis. Although the exact mechanism of internalization is not known at this time, intracellular punctate fluorescence suggests an endosomal pathway that acidifies the molecules as they transit from early (higher pH) to late (lower pH) endosomes/lysosomes. In contrast, protonation of LS662 appears to facilitate internalization by a process that is less dependent on active transport. We postulate that the positively charged LS662 interacts electrostatically with the phosphate groups on the cell membrane to induce internalization by energy-dependent and independent mechanisms similar to that of HIV tat-peptides or amphiphilic polymers.[43, 44]

Internalization of both protonated and nonprotonated forms of LS662 in cells by different mechanisms could lead to sporadic uptake of this molecular probe in many cells *in vivo*. However, our small animal imaging results indicate a high tumor selectivity demonstrated in three different cancer models. Accumulation in both the extracellular acidic space and in tumor cells provides a two-prong reporting strategy in which relatively weak fluorescence in tumors from molecules protonated in the extracellular space is visible within 1 h, followed by highly intense fluorescence induced by both intra-and extra-cellular protonation of LS662. Two-photon and SHG imaging also show that LS662 does not stain elastin and

collagen fibers in the tumor matrix, a further indication of pH-associated selective uptake in tumor tissue.

Accurate sensing of pHe *in vivo* could be advantageous in monitoring tumor growth and cell death during therapy. Our results show that LS662 accumulates in a variety of cancer models, regardless of tumor origin. Comparison of LS662 uptake in these tumor models suggests that LS662 fluorescence may correlate with the differences in pHe and the distribution of the excreted protons (Figure 4). Diffuse and invasive tumors such as PyMT[45] release protons into a large tissue volume, which could result in a more neutral physiologic pHe than implanted tumors such as 4T1/luc and A431, which could exhibit lower pHe because protons are released in small, encapsulated tissue volume. If validated with reference standards, the relative fluorescence of LS662 could be used to correlate tumor invasiveness and metastatic potential with the size, proton distribution, type, and origin.[46, 47] Unlike SNARF-1,[47, 48] which requires high concentrations for pH sensing in the visible light region, the NIR emission of LS662 allows the interrogation of tumor tissues noninvasively in small animals with higher detection sensitivity using relatively lower dose of the molecular probe.

In summary, LS662 is a promising small molecule for reporting cellular and extracellular pH of tumors. Its capacity to illuminate the tumors within 1 h, prolonged retention in tumors, and NIR fluorescence is useful for diverse biomedical applications, including the targeted delivery of drugs. Low background NIR fluorescence before protonation improves tumor contrast *in vivo*. This molecular probe is also capable of sensing different stages of cell death, with over a five thousand-fold fluorescence increase in dying and dead tumor cells because of the elevated acidity of necrotic or apoptotic tumor bodies.[34, 35] This work has unveiled a novel class of small molecules that can target diseased tissue simply through electrostatic changes produced by environmental factors.

Supplementary Material

Refer to Web version on PubMed Central for supplementary material.

Acknowledgments

This project was supported in part by funds from the US National Institutes of Health (NIH) NCI (P50 CA094056 and R01 CA171651), NIBIB (R01 EB007276 and R01 EB008111), and shared instrumentation grants (S10 OD016237 and S10 RR031625), as well as a grant from the National Science Foundation (CCF 0963742). RCG is partially supported by the Mr. and Mrs. Spencer T. Olin Fellowship for Women in Graduate Study. We thank Mark Miller and the In Vivo Imaging Core at Washington University School of Medicine for technical support and the use of multiphoton microscopy system. We thank Joseph Ippolito for preparing the MES and HEPES buffers at different pHs.

References

1. Cardone RA, Casavola V, Reshkin SJ. The role of disturbed pH dynamics and the Na+/H+ exchanger in metastasis. Nat Rev Cancer. 2005; 5(10):786–95. [PubMed: 16175178]
2. Gillies RJ, Raghunand N, Karczmar GS, Bhujwalla ZM. MRI of the tumor microenvironment. J Magn Reson Imaging. 2002; 16(4):430–50. [PubMed: 12353258]

3. Robey IF, Baggett BK, Kirkpatrick ND, Roe DJ, Dosescu J, Sloane BF, Hashim AI, Morse DL, Raghunand N, Gatenby RA, Gillies RJ. Bicarbonate increases tumor pH and inhibits spontaneous metastases. Cancer research. 2009; 69(6):2260–8. [PubMed: 19276390]
4. Robey IF, Nesbit LA. Investigating mechanisms of alkalinization for reducing primary breast tumor invasion. Biomed Res Int. 2013; 2013:485196. [PubMed: 23936808]
5. Wu F, Guo NJ, Tian H, Marohn M, Gearhart S, Bayless TM, Brant SR, Kwon JH. Peripheral blood microRNAs distinguish active ulcerative colitis and Crohn's disease. Inflamm Bowel Dis. 2011; 17(1):241–50. [PubMed: 20812331]
6. Raghunand N, He X, Sluis R, Mahoney B, Baggett B, Taylor C, Paine-Murrieta G, Roe D, Bhujwalla Z, Gillies R. Enhancement of chemotherapy by manipulation of tumor pH. Brit J Cancer. 1999; 80(7):6. [PubMed: 10466754]
7. Muller V, Riethdorf S, Rack B, Janni W, Fasching PA, Solomayer E, Aktas B, Kasimir-Bauer S, Zeitz J, Pantel K, Fehm T. group Ds. Prospective evaluation of serum tissue inhibitor of metalloproteinase 1 and carbonic anhydrase IX in correlation to circulating tumor cells in patients with metastatic breast cancer. Breast Cancer Res. 2011; 13(4):R71. [PubMed: 21745383]
8. Neri D, Supuran CT. Interfering with pH regulation in tumours as a therapeutic strategy. Nat Rev Drug Discov. 2011; 10(10):767–77. [PubMed: 21921921]
9. Robey IF, Martin NK. Bicarbonate and dichloroacetate: evaluating pH altering therapies in a mouse model for metastatic breast cancer. BMC Cancer. 2011; 11:235. [PubMed: 21663677]
10. Webb BA, Chimenti M, Jacobson MP, Barber DL. Dysregulated pH: a perfect storm for cancer progression. Nat Rev Cancer. 2011; 11(9):671–7. [PubMed: 21833026]
11. Lee H, Akers W, Bhushan K, Bloch S, Sudlow G, Tang R, Achilefu S. Near-infrared pH-activatable fluorescent probes for imaging primary and metastatic breast tumors. Bioconjug Chem. 2011; 22(4):777–84. [PubMed: 21388195]
12. Urano Y, Asanuma D, Hama Y, Koyama Y, Barrett T, Kamiya M, Nagano T, Watanabe T, Hasegawa A, Choyke PL, Kobayashi H. Selective molecular imaging of viable cancer cells with pH-activatable fluorescence probes. Nat Med. 2009; 15(1):104–9. [PubMed: 19029979]
13. Ogawa M, Kosaka N, Regino CA, Mitsunaga M, Choyke PL, Kobayashi H. High sensitivity detection of cancer in vivo using a dual-controlled activation fluorescent imaging probe based on H-dimer formation and pH activation. Mol Biosyst. 2010; 6(5):888–93. [PubMed: 20567775]
14. Chan KWY, Liu G, Song X, Kim H, Yu T, Arifin DR, Gilad AA, Hanes J, Walczak P, van Zijl PCM, Bulte JWM, McMahon MT. MRI-detectable pH nanosensors incorporated into hydrogels for in vivo sensing of transplanted-cell viabillity. Nat Materials. 2013; 12:7.
15. Kogan F, Haris M, Singh A, Cai K, Debrosse C, Nanga RP, Hariharan H, Reddy R. Method for high-resolution imaging of creatine in vivo using chemical exchange saturation transfer. Magn Reson Med. 2014; 71(1):164–72. [PubMed: 23412909]
16. Rivlin M, Horev J, Tsarfaty I, Navon G. Molecular imaging of tumors and metastases using chemical exchange saturation transfer (CEST) MRI. Sci Rep. 2013; 3:3045. [PubMed: 24157711]
17. Liu Y, Bauer AQ, Akers WJ, Sudlow G, Liang K, Shen D, Berezin MY, Culver JP, Achilefu S. Hands-free, wireless goggles for near-infrared fluorescence and real-time image-guided surgery. Surgery. 2011; 149(5):689–98. [PubMed: 21496565]
18. Kaijzel EL, van Heijningen PM, Wielopolski PA, Vermeij M, Koning GA, van Cappellen WA, Que I, Chan A, Dijkstra J, Ramnath NW, Hawinkels LJ, Bernsen MR, Lowik CW, Essers J. Multimodality imaging reveals a gradual increase in matrix metalloproteinase activity at aneurysmal lesions in live fibulin-4 mice. Circ Cardiovasc Imaging. 2010; 3(5):567–77. [PubMed: 20592247]
19. Sheth RA, Upadhyay R, Stangenberg L, Sheth R, Weissleder R, Mahmood U. Improved detection of ovarian cancer metastases by intraoperative quantitative fluorescence protease imaging in a pre-clinical model. Gynecol Oncol. 2009; 112(3):616–22. [PubMed: 19135233]
20. Jaffer FA, Kim DE, Quinti L, Tung CH, Aikawa E, Pande AN, Kohler RH, Shi GP, Libby P, Weissleder R. Optical visualization of cathepsin K activity in atherosclerosis with a novel, protease-activatable fluorescence sensor. Circulation. 2007; 115(17):2292–8. [PubMed: 17420353]

21. Jaffer FA, Vinegoni C, John MC, Aikawa E, Gold HK, Finn AV, Ntziachristos V, Libby P, Weissleder R. Real-time catheter molecular sensing of inflammation in proteolytically active atherosclerosis. Circulation. 2008; 118(18):1802–9. [PubMed: 18852366]
22. Barnett EM, Zhang X, Maxwell D, Chang Q, Piwnica-Worms D. Single-cell imaging of retinal ganglion cell apoptosis with a cell-penetrating, activatable peptide probe in an in vivo glaucoma model. Proc Natl Acad Sci USA. 2009; 106(23):9391–6. [PubMed: 19458250]
23. Klohs J, Baeva N, Steinbrink J, Bourayou R, Boettcher C, Royl G, Megow D, Dirnagl U, Priller J, Wunder A. In vivo near-infrared fluorescence imaging of matrix metalloproteinase activity after cerebral ischemia. J Cereb Blood Flow Metab. 2009; 29(7):1284–92. [PubMed: 19417756]
24. Maxwell D, Chang Q, Zhang X, Barnett EM, Piwnica-Worms D. An improved cell-penetrating, caspase-activatable, near-infrared fluorescent peptide for apoptosis imaging. Bioconjug Chem. 2009; 20(4):702–9. [PubMed: 19331388]
25. Hilderbrand SA, Kelly KA, Niedre M, Weissleder R. Near infrared fluorescence-based bacteriophage particles for ratiometric pH imaging. Bioconjug Chem. 2008; 19(8):1635–9. [PubMed: 18666791]
26. Panizzi P, Nahrendorf M, Wildgruber M, Waterman P, Figueiredo JL, Aikawa E, McCarthy J, Weissleder R, Hilderbrand SA. Oxazine conjugated nanoparticle detects in vivo hypochlorous acid and peroxynitrite generation. Journal of the American Chemical Society. 2009; 131(43):15739–44. [PubMed: 19817443]
27. Smith MCP, Luker KE, Garbow JR, Prior JL, Jackson E, Piwnica-Worms D, Luker GD. CXCR4 Regulates Growth of Both Primary and Metastatic Breast Cancer. Cancer research. 2004; 64:8604–8612. [PubMed: 15574767]
28. Chen X, Nadiarynkh O, Plotnikov S, Campagnola PJ. Second harmonic generation microscopy for quantitative analysis of collagen fibrillar structure. Nat Protoc. 2012; 7(4):654–69. [PubMed: 22402635]
29. Mansfield J, Yu J, Attenburrow D, Moger J, Tirlapur U, Urban J, Cui Z, Winlove P. The elastin network: its relationship with collagen and cells in articular cartilage as visualized by multiphoton microscopy. J Anat. 2009; 215(6):682–91. [PubMed: 19796069]
30. Angiari S, Rossi B, Piccio L, Zinselmeyer BH, Budui S, Zenaro E, Della Bianca V, Bach SD, Scarpini E, Bolomini-Vittori M, Piacentino G, Dusi S, Laudanna C, Cross AH, Miller MJ, Constantin G. Regulatory T cells suppress the late phase of the immune response in lymph nodes through P-selectin glycoprotein ligand-1. J Immunol. 2013; 191(11):5489–500. [PubMed: 24174617]
31. Zhang Z, Achilefu S. Design, synthesis and evaluation of near-infrared fluorescent pH indicators in a physiologically relevant range. Chem Commun (Camb). 2005; (47):5887–9. [PubMed: 16317464]
32. Keilin DHEF. Cytochrome and cytochrome oxidase. Proceedings of the Royal Society of London Series B, Biological Sciences. 1939; 127:167–191.
33. Cao W, Zheng W, Chen T. Ruthenium polypyridyl complex inhibits growth and metastasis of breast cancer cells by suppressing FAK signaling with enhancement of TRAIL-induced apoptosis. Scientific reports. 2015; 5:9157. [PubMed: 25778692]
34. Shrode LM, Tapper H, Grinstein S. Role of Intracellular pH in Proliferation, Transformation, and Apoptosis. J Bioenerg Biomembr. 1997; 29(4):7.
35. Casey JR, Grinstein S, Orlowski J. Sensors and regulators of intracellular pH. Nature reviews Molecular cell biology. 2010; 11(1):50–61. [PubMed: 19997129]
36. Patwardhan S, Bloch S, Achilefu S, Culver J. Time-dependent whole-body fluorescence tomography of probe bio-distributions in mice. Optics Express. 2005; 13(7):14.
37. Guo J, Du C, Shan L, Zhu H, Xue B, Qian Z, Achilefu S, Gu Y. Comparison of near-infrared fluorescent deoxyglucose probes with different dyes for tumor diagnosis in vivo. Contrast media & molecular imaging. 2012; 7(3):289–301. [PubMed: 22539399]
38. Achilefu S, Dorshow R, Bugai JRR. Novel receptor-targeted fluorescent contrast agents for in vivo tumor imaging. Invest Radiol. 2000; 35(8):6.
39. Helmchen F, Denk W. Deep tissue two-photon microscopy. Nat Meth. 2005; 2(12):932–940.

40. Zoonens M, Reshetnyak YK, Engelman DM. Bilayer interactions of pHLIP, a peptide that can deliver drugs and target tumors. Biophys J. 2008; 95(1):225–35. [PubMed: 18359793]

41. Wang Y, Zhou K, Huang G, Hensley C, Uange X, Ma X, Zhao T, Sumer BD, DeBerardinis RJ, Gao J. A nanoparticle-based strategy for the imaging of a broad range of tumours by nonlinear amplification of microenvironment signals. Nat Materials. 2013

42. Yang J. Stimuli-responsive drug delivery systems. Adv Drug Deliv Rev. 2012; 64(11):965–6. [PubMed: 22580333]

43. Madani F, Lindberg S, Langel U, Futaki S, Graslund A. Mechanisms of cellular uptake of cell-penetrating peptides. J Biophys. 2011; 2011:414729. [PubMed: 21687343]

44. Palermo EF, Kuroda K. Structural determinants of antimicrobial activity in polymers which mimic host defense peptides. Applied microbiology and biotechnology. 2010; 87(5):1605–15. [PubMed: 20563718]

45. Lin EY, Jones JG, Li P, Zhu L, Whitney KD, Muller WJ, Pollard JW. Progression to Malignancy in the Polyoma Middle T Oncoprotein Mouse Breast Cancer Model Provides a Reliable Model for Human Diseases. Amer J Path. 2003; 163(5):2113–2126. [PubMed: 14578209]

46. Gatenby RA, Gawlinski ET, Gmitro AF, Kaylor B, Gillies RJ. Acid-mediated tumor invasion: a multidisciplinary study. Cancer research. 2006; 66(10):5216–23. [PubMed: 16707446]

47. Estrella V, Chen T, Lloyd M, Wojtkowiak J, Cornnell HH, Ibrahim-Hashim A, Bailey K, Balagurunathan Y, Rothberg JM, Sloane BF, Johnson J, Gatenby RA, Gillies RJ. Acidity generated by the tumor microenvironment drives local invasion. Cancer research. 2013; 73(5): 1524–35. [PubMed: 23288510]

48. Tseng JC, Benink HA, McDougall MG, Chico-Calero I, Kung AL. In Vivo Fluorescent Labeling of Tumor Cells with the HaloTag Technology. Curr Chem Genomics. 2012; 6:48–54. [PubMed: 23115613]

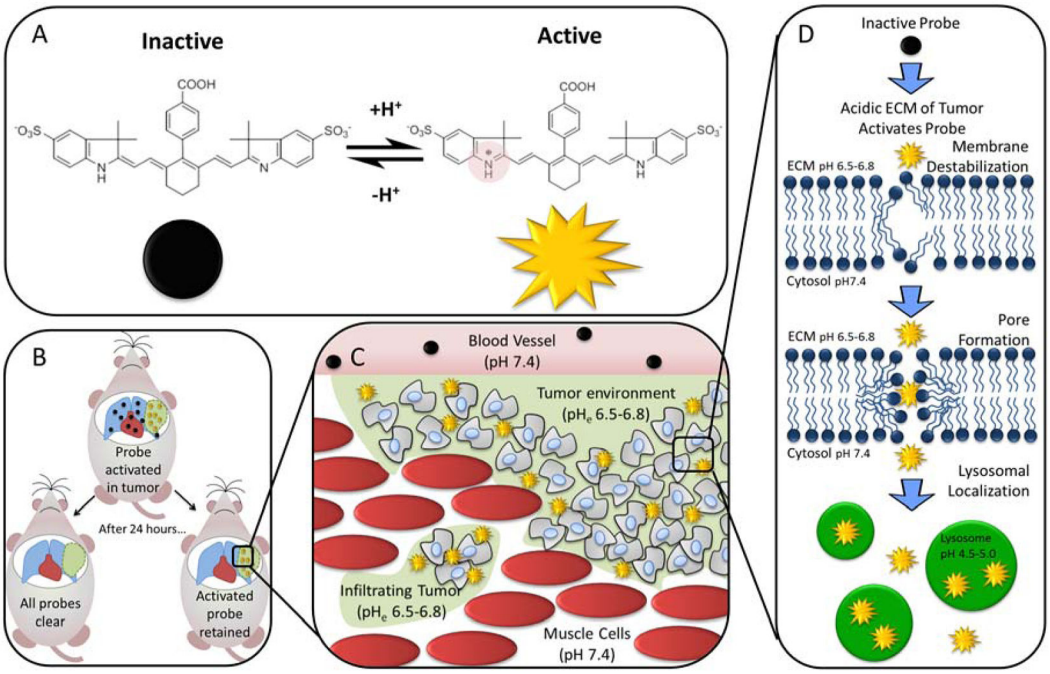

Figure 1.

(A) LS662 is a pH activated probe that becomes highly fluorescent in acidic solution. (B) *In vivo*, LS662 is activated in tumors and the inactive probe clears from uninvolved tissue, simultaneously increasing contrast and decreasing the dose of LS662 to nontumor regions. (C) LS662 selectively activates in infiltrating tumor. (D) Once LS662 is activated by the protonation of the indolium ring nitrogen, it acts as an amphiphilic small molecules that can penetrate into tumor cells by destabilization of the cell membrane. Once, inside the cell, it can be seen activated in the acidic lysosomes.

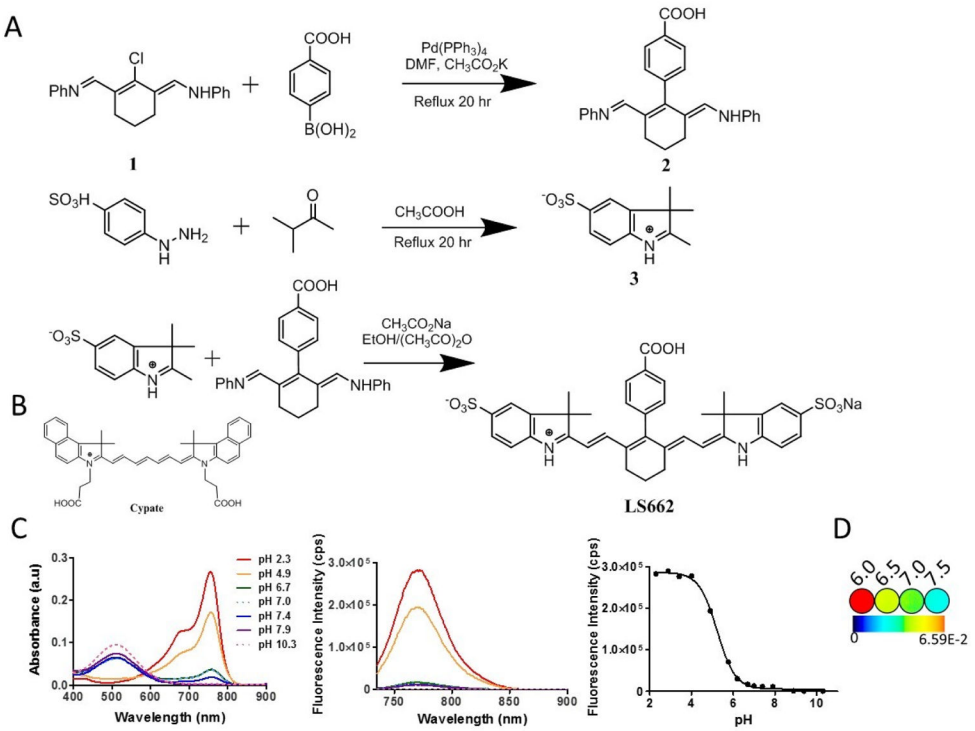

Figure 2.

(A) Synthesis route of LS662. (B) Chemical structure of cypate. (C) Absorption and emission spectra of pH titrated LS662 in water from pH 2–10. Absorption in basic solution primarily occurs in the visible range, while absorption in acid solution occurs in the NIR. In acidic solution, excitation at 720 nm results in fluorescence at 758 nm. LS662 has a pK_a of 5.2. (D) Pseudocolor images of a solution of LS662 at pH 6.0, 6.5, 7.0 and 7.5 (see methods section for solution preparation).

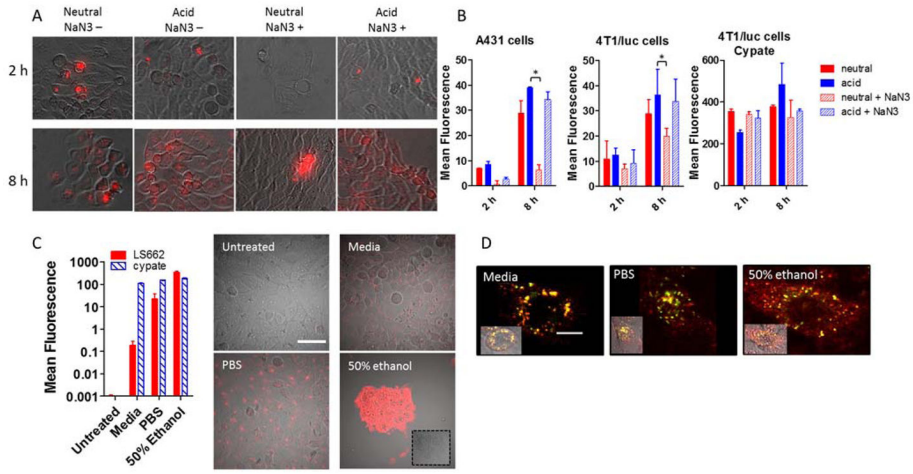

Figure 3.

(A) Images of cellular uptake of LS662 in A431 cells for 2 or 8 h at normal physiological pH 7.4 (neutral) or acidic pH 6.4 (acid) media. Sodium azide (NaN3+) was added to each condition to determine whether the internalization of LS662 is energy dependent. (B) Quantification of the cellular uptake, described in A, in A431 and 4T1/luc cells with LS662 and cypate, *p-value < 0.05. (C) Cellular uptake of LS662 and cypate in A431 cells treated in three conditions: media, PBS, and 50% ethanol, to probe healthy, dying and dead cells, respectively. The images show LS662 fluorescence; cypate images not shown. (D) Healthy, dying and dead cells were coincubated with LS662 (red) lysotracker (green), to investigate the subcellular localization of LS662. Scale bar = 10 μm.

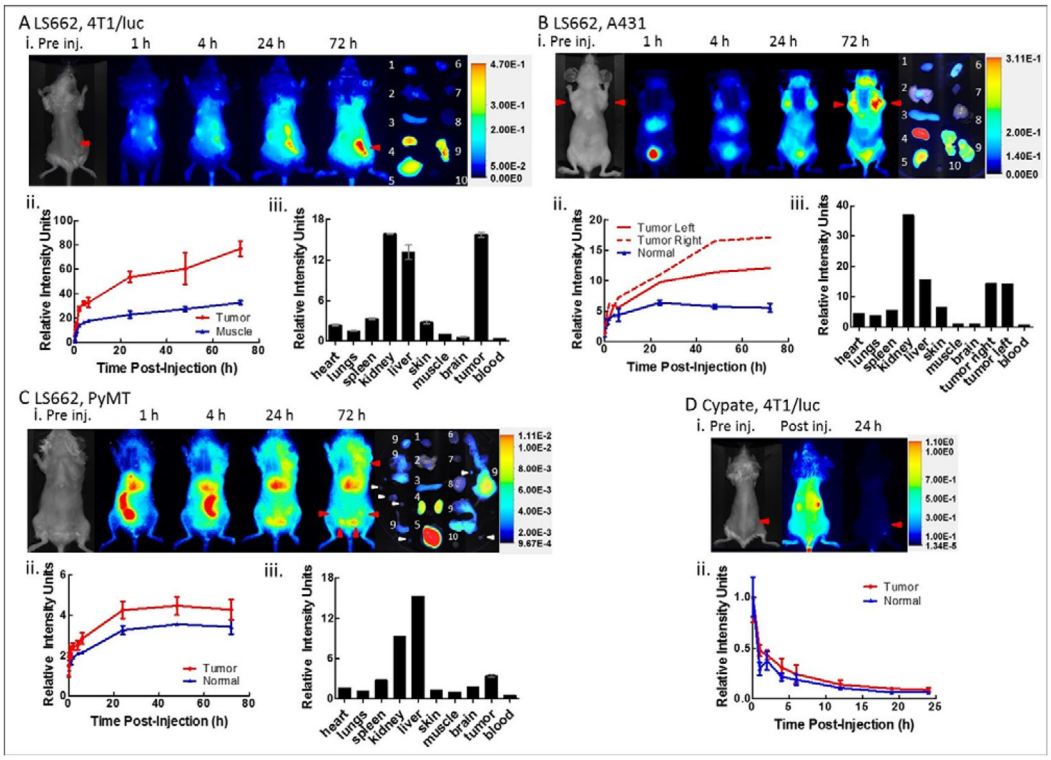

Figure 4.

(A, B, C) LS662 in 4T1/luc murine breast cancer, A, A431, human epidermal cancer, B, and PyMT spontaneous breast cancer C. (i) Fluorescence images of tumor bearing mouse at indicated times post-injection. Red arrows indicate the location of the tumor. Pre-injection image show the bright field image of the mouse. (ii) Plot of the average fluorescence values of the tumor region compared to normal tissue control region obtained from the in vivo images. The values are normalized to the post injection fluorescence intensity of each region, respectively. (iii) Fluorescence intensity in organs of interest after the mouse was sacrificed and the organs were excised. All values are normalized to the muscle signal. (D) Cypate, in 4T1/luc murine breast cancer model (n = 3). Error bars are shown for cases of n ≥ 3.

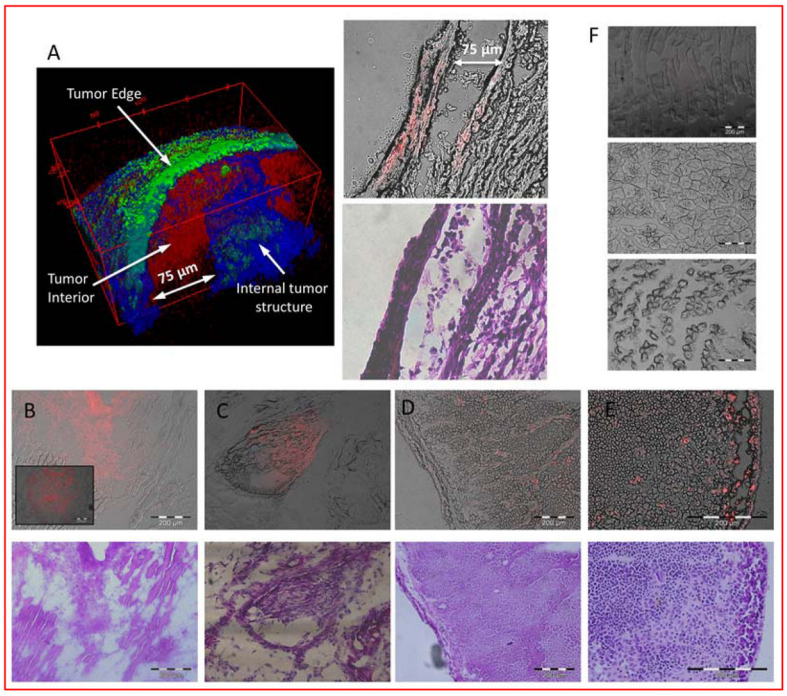

Figure 5.

(A) 2-photon tomographic reconstruction of 4T1/luc tumor, excised immediately after the animal was sacrificed, 24 h post initial injection of LS662, (Green-elastin, blue- collagen, Red-LS662.) Matching fluorescence sectioned histology showing LS662 fluorescence and H&E (B,C, D) Fluorescence (red) and H&E stained images, from a 4T1/luc, A431, and PyMT tumor, respectively. (E) Lymph node infiltrated with tumor cells shows LS662 fluorescence. (F) Muscle samples from 4T1/luc (top), A431 (middle), and PyMT (bottom) bearing mice, show no LS662 fluorescence.